

Spatial and kinematic segregation in star cluster merger remnants

David R. Cole^{1,2*}, Victor P. Debattista^{2†}, Anna-Lisa Varri^{3‡}, Markus Hartmann^{4§}
and Anil C. Seth^{5¶}

¹*Rudolf Peierls Centre for Theoretical Physics, Keble Road, Oxford, OX1 3NP, United Kingdom*

²*Jeremiah Horrocks Institute, University of Central Lancashire, Preston, PR1 2HE, United Kingdom*

³*School of Mathematics and Maxwell Institute for Mathematical Sciences, University of Edinburgh, Edinburgh, EH9 3JZ, United Kingdom*

⁴*Astronomisches Rechen-Institut, Zentrum für Astronomie der Universität Heidelberg (ZAH), Mönchhofstr. 12-14, 69120 Heidelberg, Germany*

⁵*Department of Physics and Astronomy, University of Utah, Salt Lake City, UT 84112, USA*

Accepted xxx Received xxx ; in original form 6 July 2018

ABSTRACT

Globular clusters which exhibit chemical and dynamical complexity have been suggested to be the stripped nuclei of dwarf galaxies (e.g., M54, ω Cen). We use N -body simulations of nuclear star clusters forming via the mergers of star clusters to explore the persistence of substructure in the phase space. We find that the observed level of differentiation is difficult to reconcile with the observed if nuclear clusters form wholly out of the mergers of star clusters. Only the star clusters that merged most recently retain sufficiently distinct kinematics to be distinguishable from the rest of the nuclear cluster though the critical factor is the number of merger events not the elapsed time. In situ star formation must therefore be included to explain the observed properties of nuclear star clusters, in good agreement with previous results.

Key words: galaxies: bulges — galaxies: evolution — galaxies:kinematics and dynamics — galaxies: nuclei — galaxies: structure

1 INTRODUCTION

High resolution *Hubble Space Telescope* (*HST*) observations have shown that many low to intermediate mass galaxies across the Hubble sequence contain a dense star cluster at their centre, a nuclear star cluster (NSC) (Carollo et al. 1997; Böker et al. 2002; Côté et al. 2006; Turner et al. 2012).

NSCs in late-type galaxies are found to have complex star formation histories with mean luminosity-weighted ages ranging from 10 Myr to 10 Gyr (Rossa et al. 2006). Observations frequently show that the star formation is bursty, recurring on a timescale of the order of 100 Myr with the most recent episodes in the last 100 Myr (Walcher et al. 2005, 2006). One example is the NSC in M33 which had periods of star formation 40 Myr and 1 Gyr ago (Long, Charles & Dubus 2002). Georgiev & Böker (2014) studied 228 late-type galaxies and found that recent star formation is common and their stellar populations had a

range of ages. Carson et al. (2015) found increasing roundness at longer wavelengths in *HST* WFC images of the 10 brightest and nearest NSCs. They inferred that the NSCs contained discs with younger stellar populations. Colour-colour diagrams for most of these NSCs also show evidence for two populations, a younger one of the order of a few hundred Myr old and an older one more than a Gyr old. Pfuhl et al. (2011) studied the Milky Way’s NSC and found that $\sim 80\%$ of its stars are more than 5 Gyr old but there was a deep minimum in star formation 1 to 2 Gyr ago followed by an increase in star formation in the last few hundred Myr. NSCs in late-type galaxies are often made of an older spheroidal component with a younger, bluer disc embedded in it, with the disc approximately aligned with the plane of the main galactic disc (Seth et al. 2006, 2008). The NSC in NGC 4244 has such a structure and the stars in the disc are less than 100 Myr old. Integral field spectroscopy indicates that the disc is rotating in the same sense as the main galactic disc and is misaligned by only $\sim 15^\circ$. The NSC in the elliptical galaxy FCC 277 also has the spheroid+disc structure with stars younger than those in the main galaxy (Lyubenova et al. 2013).

Two principal formation mechanisms have been proposed to explain the formation of NSCs: the

* E-mail: david.cole@physics.ox.ac.uk

† E-mail: vpdebattista@gmail.com

‡ E-mail: annalisa.varri@gmail.com

§ E-mail: hartmann@ari.uni-heidelberg.de

¶ E-mail: aseth@astro.utah.edu

Cluster	Mass $\times 10^6 M_{\odot}$	Absolute visual mag.	Half mass radius pc	[Fe/H]
ω Cen	2-5 ¹	-10.24	6.20	-1.62
47 Tuc	0.7-1.45 ^{2,3}	-9.37	3.49	-0.76
NGC 1851	0.561 ³	-8.35	1.85	-1.26
M54	1.45 ³	-9.96	3.76	-1.59
M22	0.536 ³	-8.45	3.03	-1.64
Terzan 5	$\sim 2^4$	-7.86	1.93	-0.28

Table 1. Properties of ω Cen, 47 Tuc, NGC 1851, M54, M22 and Terzan 5 from Harris (1997). ¹Meylan et al. (1995); van de Ven et al. (2006); D’Souza & Rix (2013), ²Marks & Kroupa (2010), ³Gnedin & Ostriker (1997), ⁴Lanzoni et al. (2010). Although 47 Tuc does not show any evidence of enhancement or spread in its iron abundance (see Marino et al. (2016)), we include it in this list in light of the estimated total mass, its complex light elements abundance patterns (e.g., see Cordero et al. 2014; Kućinskas, Dobrovolskas & Bonifacio 2014), and its rich internal dynamics (e.g., see Richer et al. 2013; Bianchini et al. 2013).

merging of GCs, and in situ star formation. In the GC merger scenario the GCs’ orbits decay due to dynamical friction and then they merge at the centre of galaxies (Tremaine, Ostriker & Spitzer 1975; Capuzzo-Dolcetta 1993; Miocchi et al. 2006; Capuzzo-Dolcetta & Miocchi 2008b,a; Antonini et al. 2012; Antonini 2013; Gnedin, Ostriker & Tremaine 2014). In situ star formation could occur due to a variety of mechanisms but would require a process whereby gas is driven to the nuclear regions of galaxies (Milosavljević 2004; Bekki 2007). These include the action of re-ionisation epoch radiation fields (Cen 2001) and compressive tidal fields (Emsellem & van de Ven 2008). Georgiev & Böker (2014) found that the half-light radius, r_{eff} , of their sample of NSCs increases with wavelength and argue that this could be explained if NSCs form from gas which falls to the centre and forms stars, meaning that younger populations will be more centrally concentrated than older ones. The most direct evidence for the need of in situ star formation comes from modelling the kinematic data for the NSC in NGC 4244. Simulations by Hartmann et al. (2011, see also De Lorenzi et al. (2013)) find that though the globular cluster (GC) merger scenario can reproduce many of the density and kinematic properties of NSCs, mergers give rise to a central peak in $v_{rms} = \sqrt{\sigma_{los}^2 + v_{los}^2}$, which is not observed in the data. Based on this, they conclude that less than 50% of the mass of the NSC could have been assembled from the mergers of GCs, with the majority due to in situ star formation.

Turning our attention to globular clusters, the interpretative paradigm for their formation and dynamical evolution is even more puzzling. At one time the Milky Ways GCs were thought to consist of a single stellar population, but the availability, over the past decade or so, of high quality and homogeneous photometric and spectroscopic datasets has revealed a much more complex picture of the star formation history of this class of stellar systems. In particular, there is now clear evidence that most Galactic GCs exhibit light elements abundance patterns and colour-magnitude di-

agram morphology indicative of the existence of multiple stellar populations (see e.g., Gratton, Carretta & Bragaglia 2012; Piotto et al. 2015). A number of possible scenarios have been proposed to provide an interpretation of such an ubiquitous and puzzling phenomenon, often invoking the presence of two (or more) generations of stellar populations, with several different possible sources for the gas out of which second population stars form. These sources include rapidly rotating massive stars, massive binary stars, and intermediate-mass asymptotic giant branch (AGB) stars (see e.g., Ventura et al. 2001; Prantzos & Charbonnel 2006; de Mink et al. 2009; D’Ercole et al. 2008, 2010, 2012). Alternative scenarios further elaborate on the role of the ejecta from massive interacting binaries, in the context of the formation of circumstellar disks of young, low mass stars (Bastian et al. 2013), as a possible origin for the observed abundance anomalies.

One crucial insight into this problem may arise from the investigation of the structural (see e.g., Vesperini et al. 2013) and kinematical properties (see e.g., Mastrobuono-Battisti & Perets 2013; Hénault-Brunet et al. 2015) of multiple stellar populations. Lardo et al. (2011) has studied nine Galactic GCs with Sloan Digital Sky Survey (SDSS) data, and found that there is a statistically significant spread in $u - g$ colour, corresponding to variations in the abundances of light elements, with the redder stars being more centrally concentrated than the bluer ones. They concluded that there are distinct populations which have different radial distributions. From the kinematic perspective, Richer et al. (2013) analysed the proper motions of main sequence stars in 47 Tuc by dividing them into four colour bands, assuming that the colour bands represent stars with different chemical composition. They found that the main sequence stars in 47 Tuc have anisotropic proper motions, and that such a feature is correlated with their colours. They also found that the bluest stars are also the most centrally concentrated, confirming that, also in the case of 47 Tuc, different stellar populations can be distinguished by their spatial distribution. More recently, Bellini et al. (2015) have studied the kinematic properties of multiple populations in NGC 2808 on the basis on high-precision Hubble Space Telescope proper-motion measurements, and they found that the helium-enriched populations are more radially anisotropic. All aspects of the formation, chemistry, and dynamical evolution of GCs are currently intensely debated (see e.g., Renzini et al. 2015; Bastian 2015; D’Antona et al. 2016), and only the synergy between state-of-the-art photometric (especially the *HST* UV Legacy Survey of Galactic GCs, presented by Piotto et al. 2015), spectroscopic (see Carretta 2015; Lardo et al. 2015), and proper motion (from *HST* and *Gaia*, e.g., see Watkins et al. 2015; Pancino, Bellazzini & Marinoni 2013, respectively) information will allow us to address many of these open questions.

One additional (and older) puzzle is the existence of globular clusters with significant variations in their heavy elements abundances. In this respect, evolutionary scenarios that include one or more merger events have been often formulated as a possible formation channel of these “multimetallic clusters” (van den Bergh 1996; Catelan 1997; Lee et al. 1999; Carretta et al. 2010a, 2011; Bekki & Yong 2012; Amaro-Seoane et al. 2013). The scenarios in this class have often been considered rather unlikely in the Galactic

environment, but not unrealistic in other settings, such as in interacting galaxies (e.g., the Antennae) or in the core of a dwarf galaxy (e.g., Sagittarius). In particular, it has been envisaged that GCs may come close and merge due to galaxy interactions or where GCs have fallen to the centre of the host system due to dynamical friction. Amaro-Seoane et al. (2013) investigated this process using N -body simulations and found that the radial distribution of different populations are similar to those in multimetallic GCs. In particular, they found that the distribution of stellar populations in their dynamical models had some resemblance to the observed distribution in ω Cen. However Catelan (1997) found that a merger of two GCs would produce a red giant branch with bi-modal colours and no such bimodality had been seen in Galactic GCs, which led to the conclusion that they are unlikely to be formed by mergers. Ferraro et al. (2009) has found that Terzan 5 shows bimodality in the red clump and red giant branch.

Interestingly, Galactic globular clusters that are characterised by anomalous metallicity distributions tend to be also particularly massive. These two aspects, coupled with additional signatures of dynamical complexity, have often been interpreted as possible indications that these stellar systems may be remnants of dwarf galaxies, which have been tidally stripped by the potential of the Milky Way (e.g. van den Bergh 1996; Bekki & Norris 2006). In this context, it has also been speculated that these objects are actually able to retain fast supernovae ejecta (hence the spread in heavy elements), as they were much more massive at their birth, further supporting the possibility of identifying them as nuclei of disrupted dwarf galaxies. Notable cases, as characterized by a very wide or even multi-modal metallicity distribution, include ω Cen (Lee et al. 1999; Bekki & Norris 2006; Carretta et al. 2010b), M54 (Carretta et al. 2010a; Sarajedini & Layden 1995; Siegel et al. 2007), and Terzan 5 (Ferraro et al. 2009; Origlia et al. 2011; Massari et al. 2014).

Significant intrinsic iron spreads have been measured also in M22 (Da Costa et al. 2009; Marino et al. 2009, 2011), M2 (Yong et al. 2014), NGC 1851 (Carretta et al. 2010a, 2011; Bekki & Yong 2012), and NGC 5286 (Marino et al. 2015, see their Table 10). In this context, it should also be emphasized that the analysis of GCs identified as having an intrinsic Fe spread deserves particular care, especially with respect to non-local thermodynamical equilibrium effects driven by over-ionization mechanisms in the atmosphere of AGB stars, which may lead to spurious metallicity assessments (e.g. see Lapenna et al. 2014; Mucciarelli et al. 2015).

Indeed, the half mass radii and masses of many clusters listed above are consistent with those of NSCs (see Table 1, and also Fig. 3 of Walcher et al. 2005). In particular, ω Cen has been often identified as a very peculiar star cluster, not just in consideration of its chemical complexity, but also for a number of interesting kinematical and dynamical features (such as the strong internal rotation Sollima et al. 2009; Bianchini et al. 2013), especially the possibility of the presence of a central, dynamically decoupled substructure, as revealed by the Schwarzschild model proposed by van de Ven et al. (2006). M54 is thought to be the NSC of the Sagittarius dSph and, as such, to be in the process of being stripped by the Galactic potential (but Siegel et al. 2011, find that M54 may be 2 kpc

in the foreground of the centre of the Sagittarius dSph, although this would require an unusual alignment). There is also evidence for the presence of an intermediate mass black hole in both M54 and ω Cen, which also favours them being stripped NSCs (Ibata et al. 2009; Wrobel, Greene & Ho 2011; Noyola, Gebhardt & Bergmann 2008; Miocchi 2010), although, especially in the case of ω Cen, this issue is still highly debated (Anderson & van der Marel 2010; van der Marel & Anderson 2010).

Inspired by the new recognition of chemical and dynamical complexity which seems to characterise these stellar systems, possibly at the interface between globular clusters and nuclear star clusters, we wish to perform an investigation of a number of structural, kinematical, and phase space properties of the products of numerical experiments of globular clusters mergers, as a possible formation scenario of NSCs. In particular, we wish to assess the persistence of any structural and kinematical distinction between the different components, associated with the original globular clusters, within the stellar system resulting from the merger process. An analysis, devoted to the exploration of the spatial and age differences among different mass components, has recently been presented by Perets & Mastrobuono-Battisti (2014); in the present investigation we wish to devote our attention in particular to the kinematical and dynamical properties.

To test whether different components can be distinguished spatially and kinematically in the case of GC merging, we have studied two simulations of this process. In Simulation 1, a number of GCs merge to form a larger object, while in Simulation 2 we start with a pre-existing star cluster, and then add several GCs, one at a time, to merge to the central object. We then study the spatial distributions and the kinematics of the stars originating in different GCs, and investigate how well mixed they are. The article is organised as follows: Section 2 describes the simulation methods, Section 3 describes the resultant star cluster for simulation 1 and the remnant star cluster for simulation 2, and finally Section 4 presents a discussion of our conclusions.

2 THE SIMULATIONS

Our N -body simulations were run using the efficient parallel tree code PKDGRAV (Stadel 2001) suitable for studying collisionless dynamics. Simulation S1 has not been described previously and we provide a description here. Simulation S2 was described by Hartmann et al. (2011) and we only provide a brief description of it here. Both simulations S1 and S2 evolve within a bulge model. The bulge model has a Hernquist (1990) profile:

$$\rho(r) = \frac{aM_b}{2\pi r(r+a)^3}, \quad (1)$$

where the mass, $M_b = 5 \times 10^9 M_\odot$, scale radius $a = 1.7$ kpc and is truncated at $r > 15a$ (Sellwood & Debattista 2009). The bulge is made up of 3.5×10^6 particles with masses ranging from $40 M_\odot$ at the centre to $3.9 \times 10^5 M_\odot$ further out giving increased mass resolution inside of 160 pc (Sellwood 2008). The bulge has no strong instabilities meaning that the distribution of particles remains unchanged on timescales up

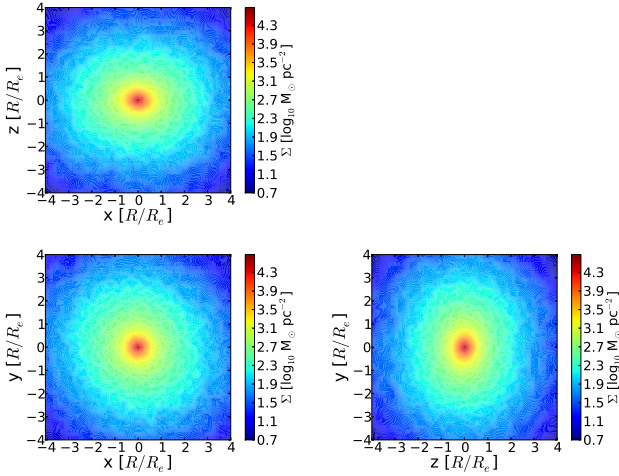


Figure 1. Surface density map of the final merger remnant from simulation 1 showing three orthogonal projections. The system has been oriented so that the resulting angular momentum is about the z-axis.

to a Gyr, more than adequate to model multiple accretions of GCs.

In simulation S1 there was no initial structure at the centre of the bulge and star clusters were placed on central orbits which decayed due to dynamical friction, falling to the centre, where six of initially ten SCs merged to form a nuclear remnant. The orbits of the ten SCs were found by selecting particles of the bulge with high angular momentum within a radius of 100 pc. We placed the SCs at the same position and with the same velocities as these bulge particles. Afterwards we rotated the SC system by 180° around the centre. The initial distances from the centre of the SCs range from 50 to 100 pc, with velocities in the range of 18 to 121 km s $^{-1}$. The model SCs have a mass of $4 \times 10^4 M_\odot$, comparable to young star clusters found in the Milky Way and the Local Group (Figer, McLean & Morris 1999; Figer et al. 2002; Mackey & Gilmore 2003; McLaughlin & van der Marel 2005). The SCs are composed of particles of equal mass of $1 M_\odot$ and softening of 0.04 pc. The SC model is a isotropic distribution function of a lowered polytrope with index $n = 2$:

$$f(x, v) \propto [-2E(x, v)]^{1/2} - [-2E_{max}]^{1/2} \quad (2)$$

An iterative process is used to produce equilibrium models (Debattista & Sellwood 2000).

Simulation S2 is the same as run A1 of Hartmann et al. (2011) which was also studied by Portaluri et al. (2013). The SC models have particles of equal mass ($15 M_\odot$) and equal softening ($\epsilon = 0.13$ pc). The concentration $c = 0.16$ is defined as $c = \log(R_{eff}/R_c)$, where $R_{eff} = 1.11$ pc is the half-mass radius (effective radius) and R_c is the core radius, where the surface density drops to half of the central. This model is also comparable to massive young star clusters in the Milky Way and the Local Group (Figer, McLean & Morris 1999; Figer et al. 2002; Mackey & Gilmore 2003; McLaughlin & van der Marel 2005). We create a NSC for the SCs to accrete onto by letting a massive star cluster of similar profile and mass 2

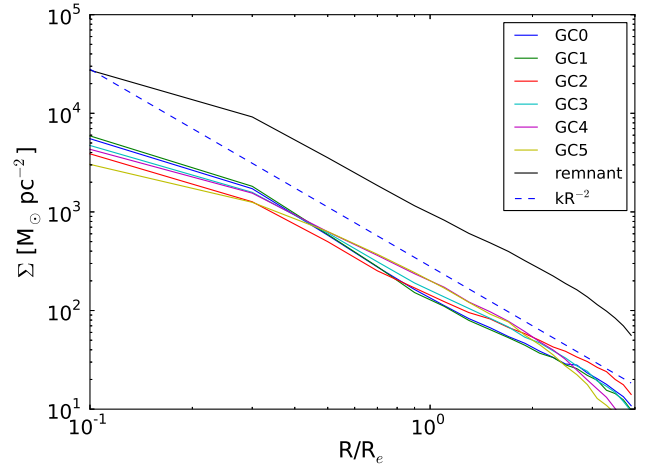


Figure 2. Cylindrical density profiles for the final merger remnant for model 1 showing the overall density and the densities contributed by stars originating in each progenitor GC. For comparison the dashed (blue) line shows a power law with an exponent of -2.

$\times 10^6 M_\odot$, $c = 0.12$ and $R_{eff} = 2.18$ pc fall to the centre of the bulge. This star cluster was allowed to settle to the centre from a circular orbit at 127 pc, which takes 65 Myr, before we started the accretion of 27 GCs, starting them on circular orbits at a distance of 32 pc from the centre. In total, the mass accreted corresponds to ~ 8.1 times the NSCs initial mass. Each accretion is allowed to finish before a new GC is inserted. A single accretion on average requires ~ 20 Myr and the 27 GCs are accreted in 810 Myr.

3 RESULTS

3.1 Properties of the the merger remnant in simulation 1

3.1.1 Final properties

In this section we examine the properties of the merger remnant formed in simulation 1 in terms of the stars which originated in each progenitor GC. The aim will be to see if we can distinguish the stars which originated in individual GCs as populations with distinct distributions and kinematics within the merger remnant.

Table 2 shows the mass and the half mass radius R_e at five times during the simulation. We measure the surface density profile at each time and find the total mass and the radius enclosing half this mass. It should be noted that there have been recent mergers at $t = 200, 400$ and 1560 Myr but not at 600 and 800 Myr which explains why there is very little change in R_e between the latter times. Figure 1 shows a map of the merger remnant's surface density within $4 R_e$ after 1.56 Gyr. It has a mass of $\sim 2.4 \times 10^5 M_\odot$ and a half mass radius $R_e \sim 3.2$ pc with a mildly oblate shape.

Figure 2 shows the density profiles and Figure 3 shows the velocity dispersion profiles in cylindrical coordinates for the merger remnant at the end of the simulation. We separate the stars by their progenitor GC and labelled the GCs in the order in which they merged, from GC0 to GC5. The contribution of each GC is distinguished as a different coloured

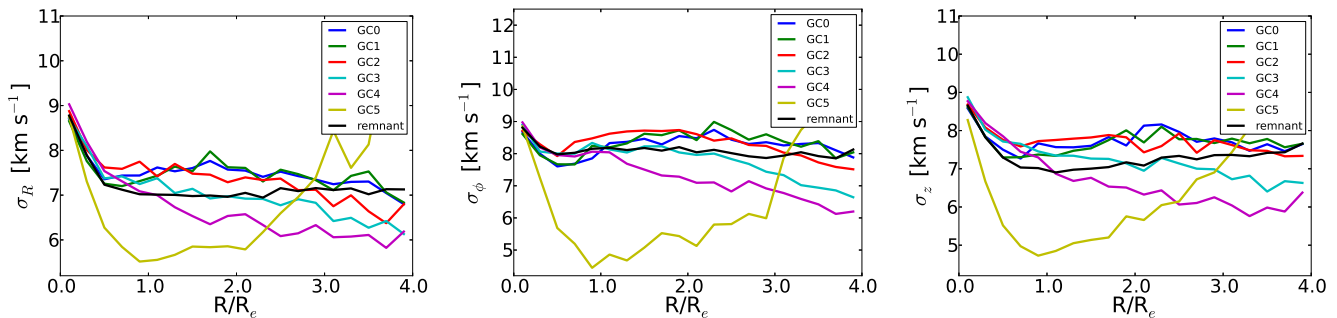


Figure 3. Velocity dispersions for the final merger remnant in model 1 at 1.56 Gyr and for the stars originating in each progenitor GC. Left: σ_R , Middle: σ_ϕ , Right: σ_z .

Time Myr	Mass $\times 10^5 M_\odot$	Half mass radius pc	N_{GC}
200	1.22	1.25	3
400	2.02	2.2	5
600	2.03	2.25	5
800	2.03	2.25	5
1560	2.4	3.2	6

Table 2. Properties of the merger remnant in simulation 1 at several times. N_{GC} is the number of globular clusters that have merged to that point.

line. It is apparent that it is difficult to identify stars visually from different progenitor GCs on the basis of the density profile and velocity dispersion, though GC5 looks distinguishable on the basis of its velocity dispersion. The final density distribution is very similar for the stars from all GCs. Even stars from the most recently merged GC5 have a very similar density profile to the stars originating in the other GCs. All velocity dispersions are similar for all the groups of stars originating in each GC except for GC5. GC5 shows the most significant deviations from the behaviour of all the other components; in particular, the radial profiles of the velocity dispersion tensor are systematically lower in the central to intermediate regions ($R < 2R_e$), while they become comparable to the values of the other components in the outer parts ($R > 2R_e$). The differences in dispersion between GCs 0, 1, 2 and 3 are $\sim 1 \text{ km s}^{-1}$ which would be hard to detect. GC4 has a maximum difference of $\sim 2 \text{ km s}^{-1}$, which may be detectable, and the maximum difference of GC5's velocity dispersion from the mean is for σ_ϕ and is $\sim 3.5 \text{ km s}^{-1}$ at $R \sim R_e$.

3.1.2 Merger remnant evolution in simulation 1

We now consider whether it is possible to distinguish different progenitor populations at earlier times in the simulation. Figure 4 shows the merger remnant density profile at 200 Myr and at 400 Myr, times at which GCs have recently merged into the remnant. When GC0, GC1 and GC2 have merged the merger remnant has a mass of $1.22 \times 10^5 M_\odot$ and a half mass-radius of $\sim 1.25 \text{ pc}$. After GC3 and GC4 have also merged the remnant's mass has increased to $2.02 \times 10^5 M_\odot$ and the half-mass radius to $\sim 2.2 \text{ pc}$. There

is a noticeably larger difference in the density profiles of the most recently merged GCs, having a flatter central density. By the time 5 GCs have merged the density profile for GC2, which was quite different from the rest when just 3 GCs had merged, has become close to the typical density profile of the other GCs.

Figure 5 shows the merger remnant velocity dispersion profiles within $4R_e$ after 3 GCs have merged and after 5 GCs have merged. These plots generally show the velocity dispersion profiles are similar in shape and magnitude for all stars originating in each GC. After 3 GCs have merged the most recently merged GC2 shows the greatest deviation from the mean at $\lesssim 3 \text{ km s}^{-1}$. After the merger of two additional GCs, it is again the most recently merged GC4 which shows lower velocity dispersions with a maximum difference of $\sim 2 \text{ km s}^{-1}$ from the mean. GC3 and GC4 are quite distinguishable here, indicating that mixing is less complete.

Figure 6 shows the evolution of the angular momentum of the merger remnant. We use Briggs figures (Briggs 1990) which are 2-D polar coordinate representations of vector directions where the two spherical angle coordinates relative to a fixed reference frame, θ and ϕ , are plotted as the radial and angle coordinates, respectively, on a 2-D polar plot. The plot shows a Briggs figure for the stars from different GCs. It can be seen that the angular momentum vectors are well aligned to better than 10° for stars inside of $4R_e$. The one exception is GC2 after 3 GCs have merged which is misaligned by $\sim 20^\circ$ from GC0 and GC1 probably due to its recent merger.

The top row in Figure 7 plots the angular momentum perpendicular to the plane of overall rotation, j_z , versus energy for stars in three spherical radial ranges at 1.56 Gyr. j_z is measured once the merger remnant has been centred and its angular momentum vector aligned with the z axis, resulting in any flattening of the stars into a disc lying in the $x-y$ plane (c.f. Figure 1). Stars in the inner radial bin have lower j_z , increasing outwards. There is no evidence of groupings of stars with distinct angular momentum signatures in these plots which would be indicative of separate populations. If we look at stars originating in different star clusters the only one that shows a significant difference in this plot is GC5,

¹ We choose this radius because Kućinskas, Dobrovolskas & Bonifacio (2014) include stars out to $4R_e$ in their work on 47 Tuc.

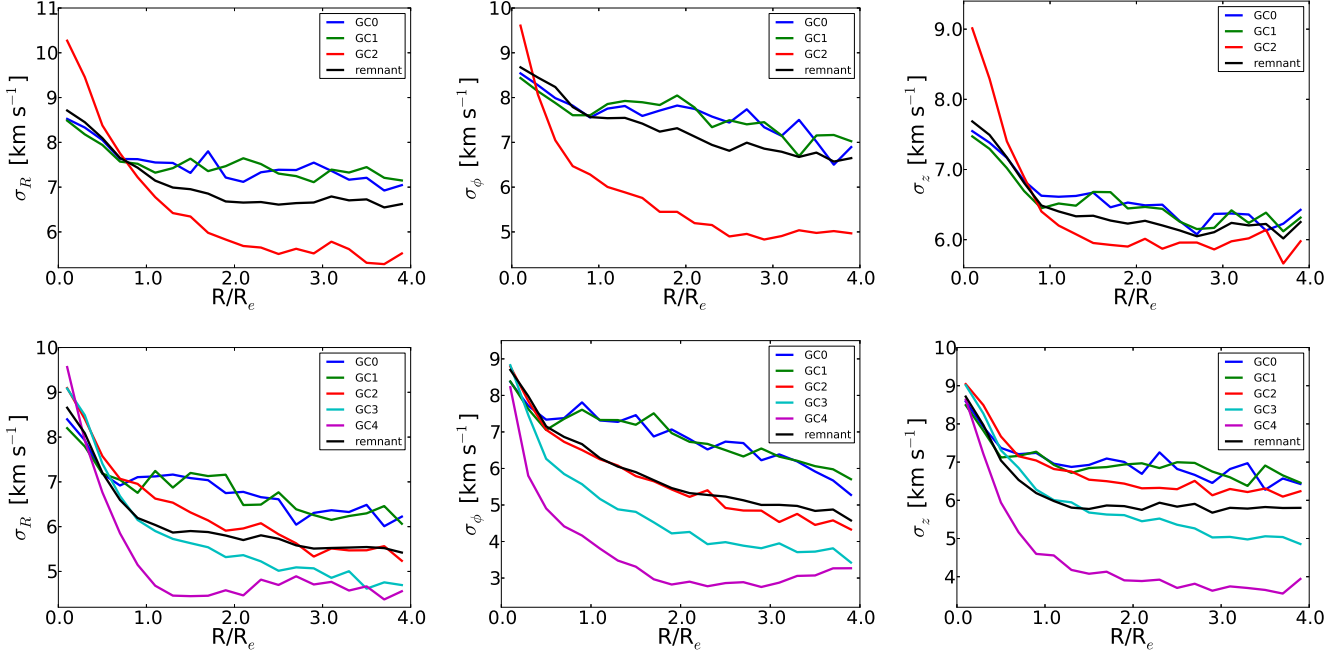


Figure 5. The velocity dispersion profile of the stars originating from individual GCs after 3 GCs have merged (top) and after 5 GCs have merged (bottom) in model 1. σ_R left, σ_ϕ middle and σ_z right.

i.e. the last one to merge. The middle and bottom rows of Figure 7 shows a comparison of j_z versus energy for GC0 and GC5 in the same 3 radial bins. GC5 shows significantly more stars with positive angular momentum in the inner two radial bins however there is still significant overlap in stellar distribution making this bias hard to observe.

Figure 8 shows the evolution of the stars from each GC on the $(V/\sigma, \epsilon)$ diagram of Binney (2005). It has been measured as described in Hartmann et al. (2011) within $2 R_e$. The radial profiles of the observables depicted in the diagram have been calculated along a line of sight corresponding to a direction perpendicular to the orientation of the angular momentum vector (i.e., edge-on). The region inside of $2 R_e$ is divided into bins of equal size and V/σ is calculated as:

$$\left(\frac{V}{\sigma}\right)_e \equiv \frac{\langle V^2 \rangle}{\langle \sigma^2 \rangle} = \frac{\sum_{n=1}^N F_n V_n^2}{\sum_{n=1}^N F_n \sigma_n^2} \quad (3)$$

and the ellipticity ϵ is found from:

$$(1 - \epsilon)^2 = q^2 = \frac{\langle y^2 \rangle}{\langle x^2 \rangle} = \frac{\sum_{n=1}^N F_n y_n^2}{\sum_{n=1}^N F_n x_n^2} \quad (4)$$

where F_n is the mass in the n th bin and V_n and σ_n are the corresponding mean velocity and velocity dispersion in that bin. It can be seen that GCs when first merged can have large differences in their location on the diagram, for instance GC2, GC4 and GC5. However as the remnant evolves, stars originating in different GCs move closer together. Even though GC2 and GC4 are initially located in very different parts of the diagram compared to the other mass components, they subsequently evolve towards the same region, corresponding to moderate flattening and mild rotation. In particular, the evolution in the diagram of GC2 (from a condition of high flattening and significant rotation) seems to be associated with merger events of GC3 and GC4. The

component GC4 evolves in a similar way, but on a longer timescale, and it becomes comparable to the other components only after the completion of all six merger events.

3.1.3 Kolmogorov-Smirnov statistics

In this section we make some quantitative measurements of the probability that stars originating in each of the GCs could be distinguished from the overall distribution by using the Kolmogorov-Smirnov (K-S) test on the fractional distribution of stars within $4 R_e$. We shall assume that stars from each of the GCs can be chemically identified and then find the probability that stars from pairs of GCs have been drawn from the same population.

We first perform K-S tests on the spatial distribution of stars from each GC at the point where 3, 5 and 6 GCs make up the merger remnant. Figure 9 shows a graphical representation of the probabilities, p (p -value), in \log_{10} space, that stars originating in pairs of merged GCs are drawn from the same population. The p -values are calculated on the cumulative fraction of a random selection of 200 stars taken 1000 times and averaged. Figure 9 is composed of n^2 cells where n is the number of GCs merged in the remnant at each time. The GCs are laid out along the x and y -axes in order and the number displayed in the cell where the appropriate row and column cross is the p -value for the probability that the stars from those two GC populations are drawn from the same population. The p -values in the upper left half of the figure (above the diagonal) are for the spatial distribution of the GCs and those in the lower right half (below the diagonal) are for the cumulative fraction of stars versus radial velocity seen by an observer viewing the system edge-on to the average plane of the GC's initial orbits. The figure is

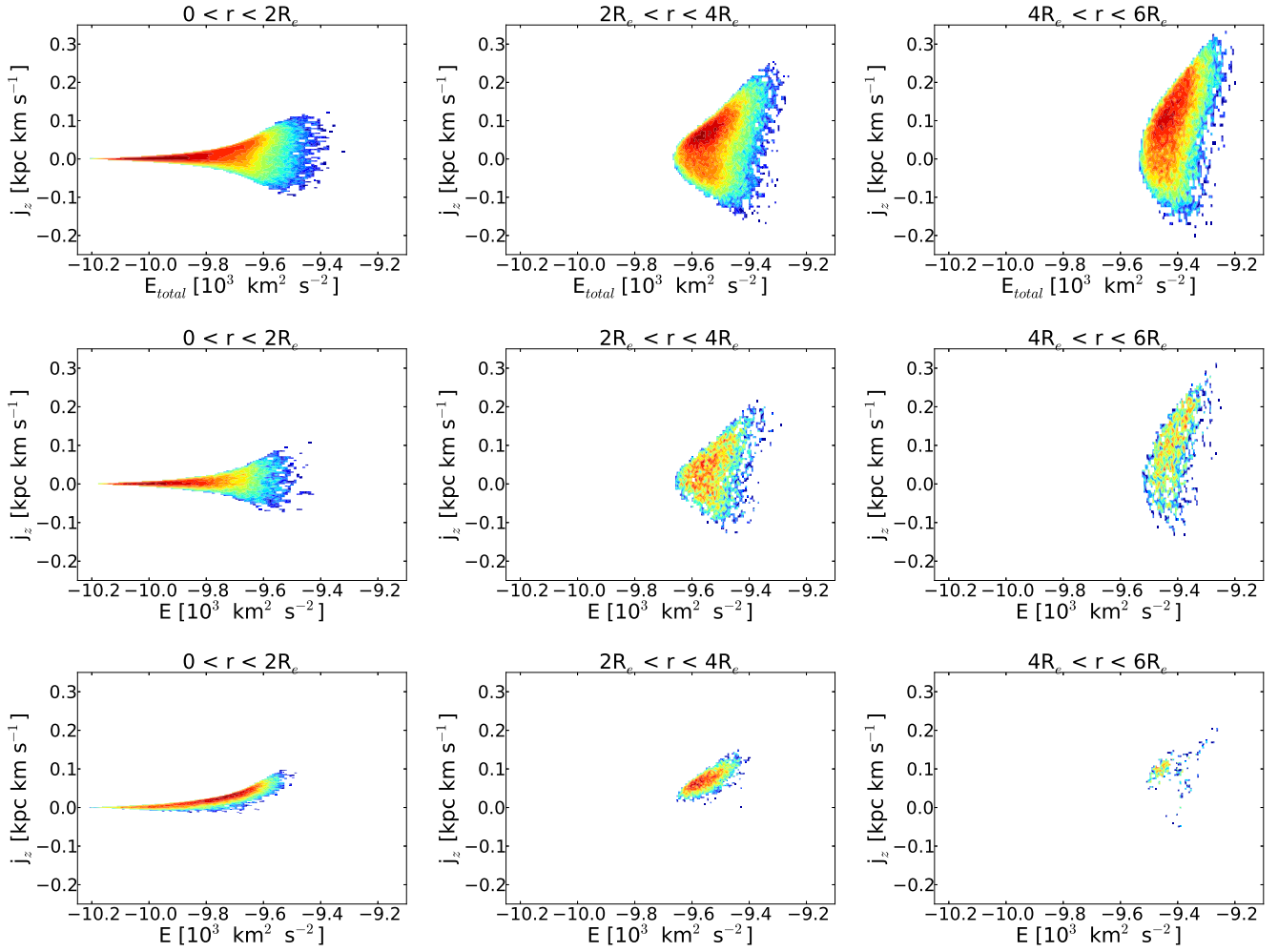


Figure 7. Plots of the vertical angular momentum j_z versus energy for stars in three radial ranges at 1.56 Gyr for simulation 1. The left column shows stars between 0 and $2 R_e$, the middle between 2 and $4 R_e$ and the right hand one shows stars between 4 and $6 R_e$. We show plots for all stars (top), for the stars originating in GC0 (middle) and GC5 (bottom). Stellar radii are measured in spherical coordinates. The number of stars in each bin in the plot is colour coded with the maximum shown in dark red and numbers decreasing moving through yellow to blue.

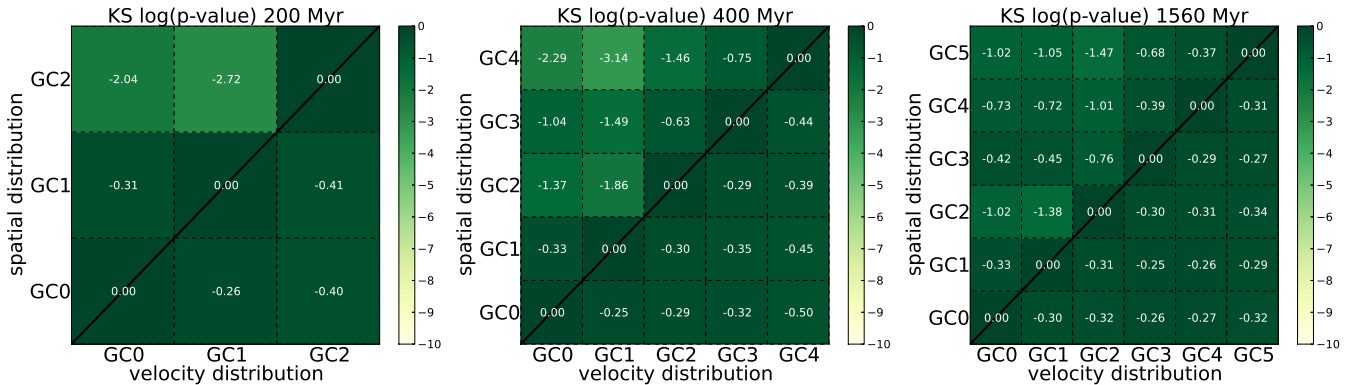


Figure 9. Model 1 \log_{10} of p -values for the cumulative spatial distribution of 200 stars within $4R_e$ when the merger remnant contains 3 GCs (left), 5 GCs (middle) and 6 GCs (right) and cumulative absolute velocity distribution as seen by an observer viewing the system edge on to the average plane of the GCs' initial orbits. The p -value for any pair of GCs is found at the intersection of the appropriate row and column. The figure is colour coded so that high p -values are darker (green) and low p -values are lighter (yellow).

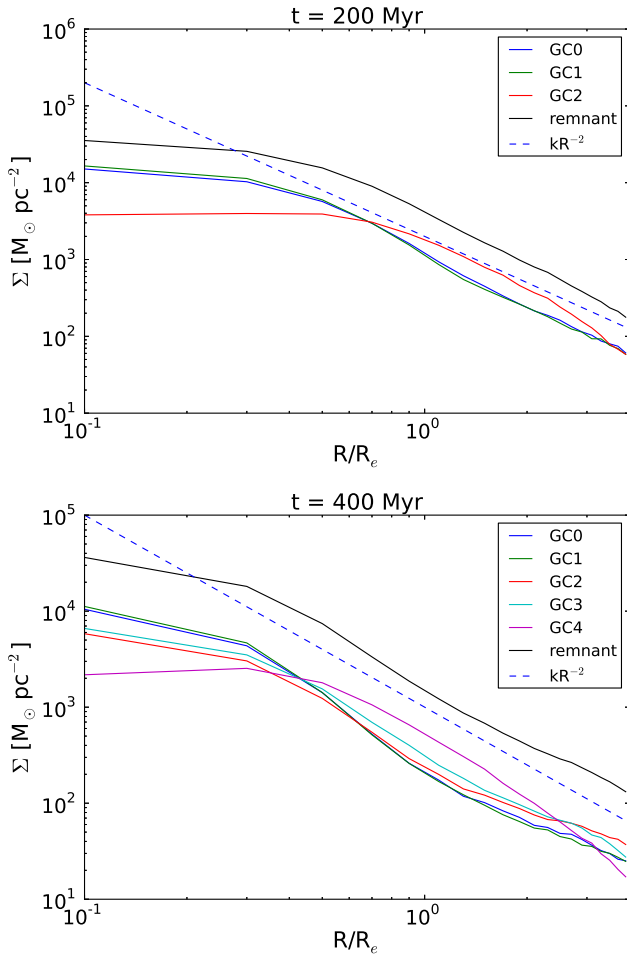


Figure 4. The density profile of the stars from individual GCs soon after a merger has occurred in model 1. Top: After 200 Myr the first three GCs have merged with GC2 being the most recent. Bottom: After 400 Myr GC3 and GC4 have now merged with GC4 being the most recent. For comparison the dashed (blue) lines show a power law relation with an exponent of -2.

colour coded so that high values of the p -value are darker (green) and low values are lighter (yellow).

The p -values for the radial velocity show that there is a high probability that any pair of GCs are drawn from the same population. The lowest value has p -value of ~ 0.32 . The p -values for the spatial distribution show a greater likelihood that two GC populations could be distinguished. When the merger remnant consists of 3 GCs GC0 and GC1 have a high probability that their stars are drawn from the same population. However the most recently merged GC2 has less than 1% probability that its stars are drawn from the same population as GC0 or GC1 so it seems possible that it could be distinguished by this method. We see a similar situation when 2 more GCs have merged, when GC4 has less than 1% probability that its stars are drawn from the same population as GC0 or GC1. However all other p -values are $>1\%$ implying that it would be difficult to distinguish separate populations. When the merger remnant contains 6 GCs even the most recently merged GC, GC5, has a greater than 2% probability that its stars are drawn from the same population as GC2. Other p -values are >0.1 apart from GC2 which

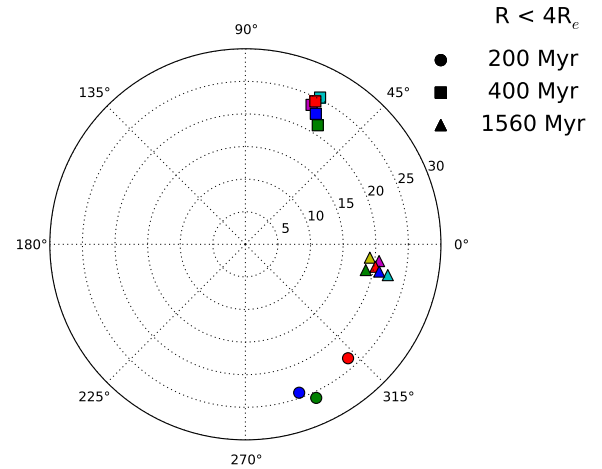


Figure 6. Briggs figure for the stars from different GCs in model 1. The direction of the angular momentum vector for each GC is indicated by the position of the symbol on the plot. Circles are values after 3 GCs have merged, squares after 5 GCs have merged and triangles after 6 GCs have merged. The plot shows the values for stars inside of $4R_e$. We use the same colour code as in other figures: GC0 blue, GC1 green, GC2 red, GC3 cyan, GC4 magenta, GC5 yellow.

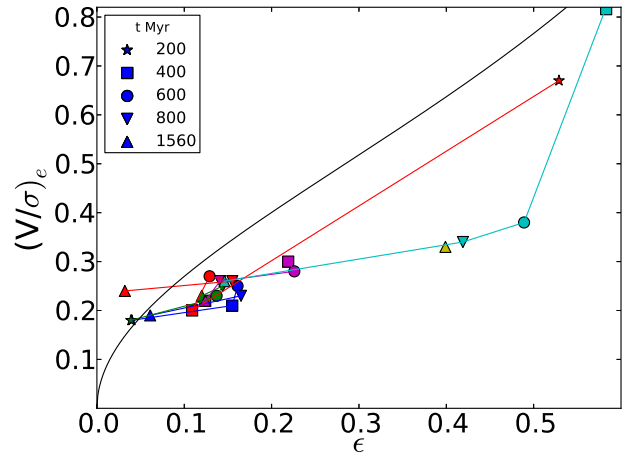


Figure 8. Evolution of the merger remnant of model 1 on the $(V/\sigma_e, \epsilon)$ diagram of Binney (2005) measured as in Hartmann et al. (2011) within $2R_e$. The black line shows the location of edge-on oblate isotropic models. Each GC is indicated by a different colour. GC0 is blue, GC1 is green, GC2 is red, GC3 is magenta, GC4 is cyan and GC5 is yellow. The different symbols show the values at different times. Note that GC3 and GC4 have not merged until 400 Myr and have no data for 200 Myr, and GC5 has just merged at the end of the simulation and shows no evolution.

remains the most distinguishable of the remaining GCs in its spatial distribution having a 4% probability that its stars are drawn from the same population as GC1.

3.2 Properties of the merger remnant in model 2

We now examine the results for model 2 (run A1 of Hartmann et al. (2011)). In this simulation a massive star cluster is placed on an orbit close to the centre where it

Time Myr	Mass $\times 10^5 M_{\odot}$	Half mass radius pc	N_{GC}
310	16.22	2.9	10
600	28.39	6.2	20
810	36.89	6.95	27

Table 3. Properties of the merger remnant in model 2 at three stages of its evolution.

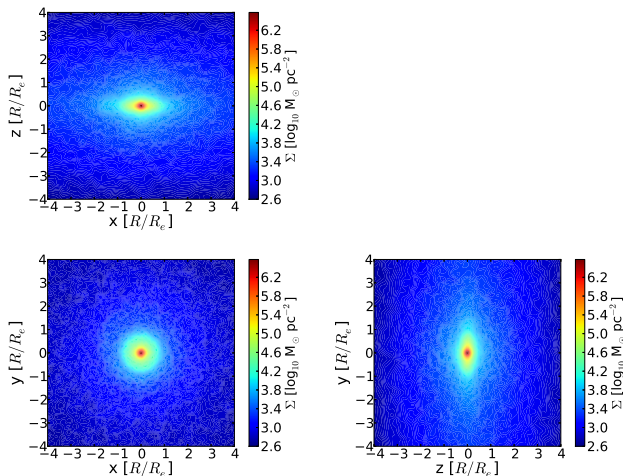


Figure 10. Surface density map of the merger remnant from model 2 (run A1 of Hartmann et al. (2011)) showing three orthogonal projections. The lower left hand plot is face-on to the plane of the orbits of the GCs and the other 2 are perpendicular to it.

eventually settles. A series of less massive star clusters are then placed on orbits at 32 pc from the centre, one at a time. Their orbits decay to the centre where they merge with the central structure. Each one is allowed to merge before the next one is added to the simulation. At the end of the simulation 27 GCs have merged. Figure 10 shows a stellar density map for model 2 at the end of the simulation. The merger remnant is much more flattened than that in simulation 1 because the GC orbits are all co-planar (compare with Figure 2). Table 3 shows the mass and half mass radius for the merger remnant at 310 Myr, 600 Myr and 810 Myr when 10, 20 and 27 clusters have merged. R_e grows significantly between 310 Myr and 600 Myr from 2.9 pc to 6.2 pc.

Figure 11 shows the evolution of the surface density profile for the merger remnant within $4R_e$ showing increasing density at the centre. Figure 12 shows surface density profiles for specific GCs at the same three times. The GCs which merge first have very similar density profiles but we see larger differences for the most recently merged GCs, especially at later times. The density profile for these GCs is either flat in the middle or even dropping towards the centre, showing that their density profiles will evolve further.

Figure 13 depicts the velocity dispersion profiles for the same GCs at the three times shown in Figs. 11 and 12 as well as the velocity dispersion for the whole cluster. These profiles show a similar pattern to the density and kinematic profiles. The first 5 GCs to merge have very similar profiles and the most recent GC to have merged always shows the

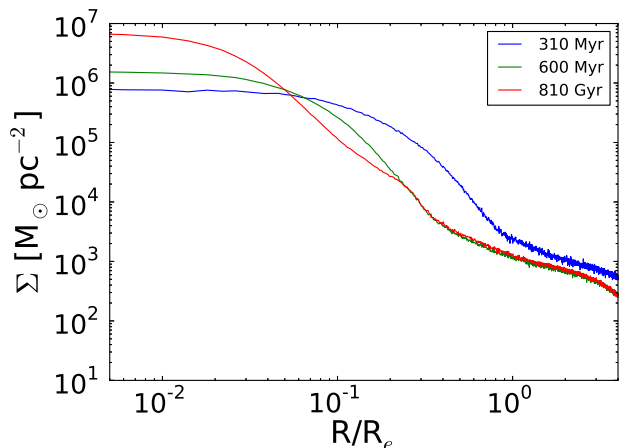


Figure 11. Evolution of the surface density for the merger remnant in model 2.

biggest difference. There are also bigger differences for the recently merged GCs at later times. The velocity dispersions for the whole cluster increase significantly from when the merger remnant contains 10 GCs to when it has 27 GCs.

At each time the 5 most recently merged GCs all show a greater difference in density profile and kinematics from the average. From inspection of the density profiles it appears that these components are still experiencing significant evolution, and therefore it is not surprising to notice some differences in their kinematics. After the first ten merger events, only the last cluster component (GC9) is still distinguishable from the global behaviour. Similarly, after twenty merger events, the behaviour of the last five clusters still retains some differences from the one of the previously merged components (especially in the case of GC19). This applies also to the subsequent components in the remnant, after it has experienced the full series of 27 merger events. It appears that in model 2 there is a greater likelihood that we would be able to distinguish individual populations from specific recently merged GCs.

3.2.1 Kolmogorov-Smirnov statistics

We performed K-S tests for model 2, looking at the spatial distribution of stars originating in individual merged GCs after 10, 20 and 27 GCs have merged, drawing 200 stars in each sample. Figure 14 shows a representative sample of cumulative fractions of stars originating in individual merged GCs at the same times considered in Figure 14. The pairs are defined by considering a selection of components which belong to either one of the 5 earliest merged GCs or from one of the 5 most recently merged clusters; such a prescription allowed us to perform a comparison between the most similar and the most different distributions, respectively. The pair from the 5 earliest merged GCs were chosen to have the greatest apparent difference in distribution. After 20 GCs have merged and 27 GCs have merged a further GC was chosen from an intermediate merger event to sample a different stage of the merger. The objective of this selection is to show the outliers of the possible comparisons in spatial segregation.

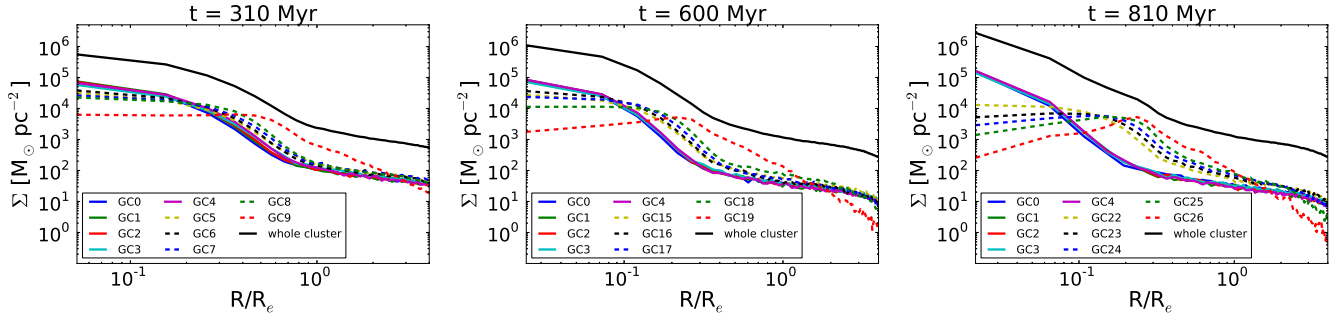


Figure 12. The density profile at three different times for model 2. The panels show when 10 GCs in the merger remnant on the left, 20 GCs in the remnant in the centre and 27 GCs in the remnant on the right.

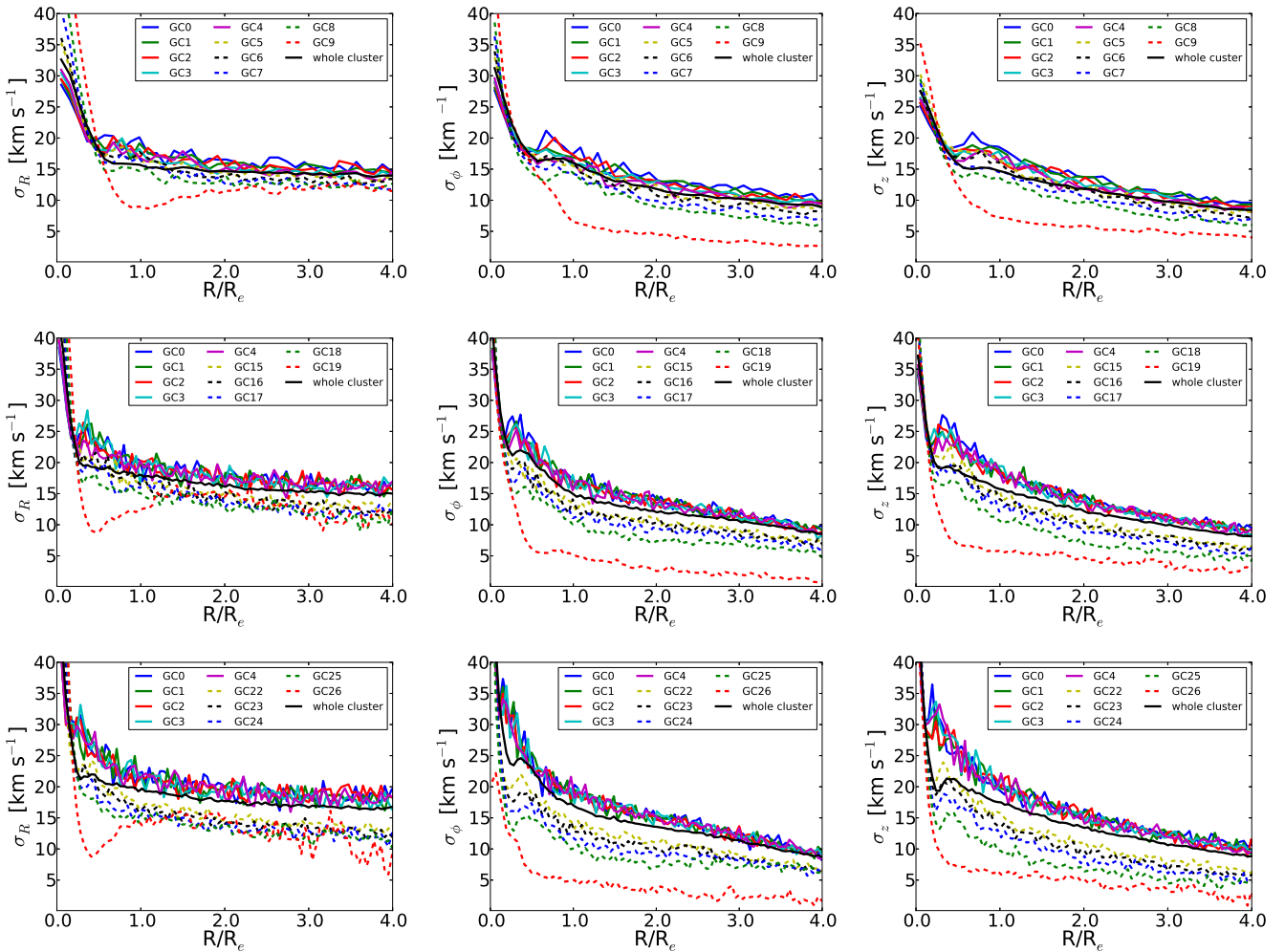


Figure 13. Model 2 velocity dispersion profiles in cylindrical coordinates when the merger remnant contains 10 GCs (top), 20 GCs (middle) and 27 GCs (bottom) for model 2. Profiles for the first 5 GCs to merge and the 5 most recently merged GCs are shown. Radial profiles are on the left, azimuthal profiles are in the centre and vertical profiles are on the right. 10 GCs have merged with the central cluster at this time.

Again the p -values in the upper left half of the figure (above the diagonal) are for the spatial distribution of the GCs and those in the lower right half (below the diagonal) are for the radial velocity seen by an observer viewing the system edge-on to the average plane of the GC's initial orbits. The p -values for the radial velocity tests again show

that there is a high probability that any pair of GCs are indistinguishable using this K-S test. The lowest p -value ~ 0.14 which still demonstrates a high likelihood that the 2 GCs are drawn from the same population. When the merger remnant contains 10 GCs the K-S tests based on the spatial distribution show that the earliest merged GCs, which are GC0,

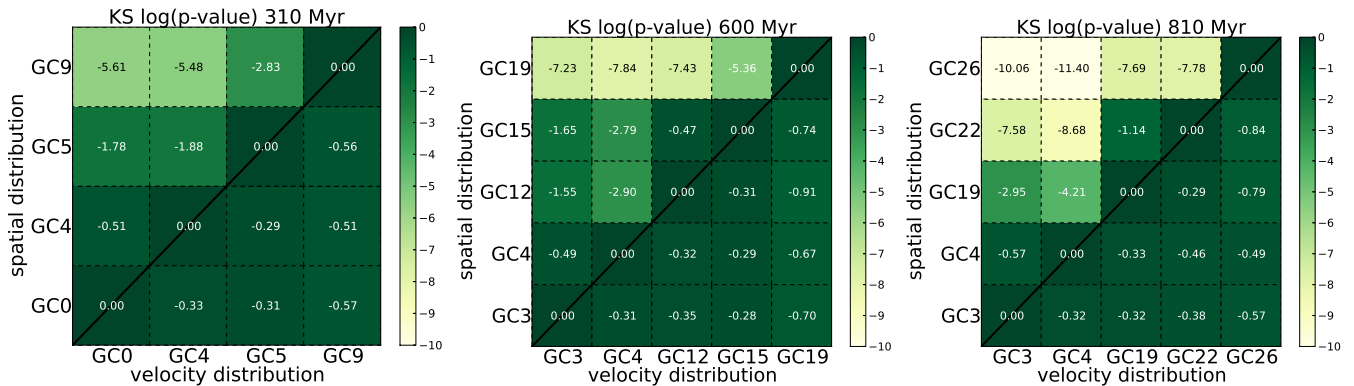


Figure 14. Model 2 \log_{10} of p -values for the cumulative spatial distribution of 200 stars within $4R_e$ when the merger remnant contains 10 GCs (left), 20 GCs (middle) and 27 GCs (right) and cumulative absolute velocity distribution as seen by an observer viewing the system edge-on to the average plane of the GCs’ initial orbits. The p -value for any pair of GCs is found at the intersection of the appropriate row and column. The figure is colour coded so that high p -values are green and low p -values are yellow.

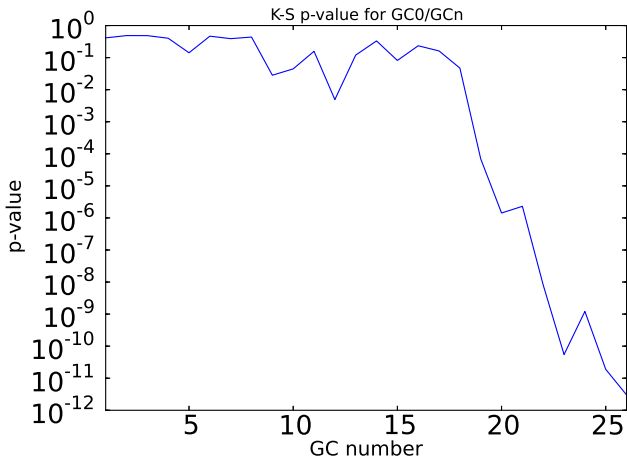


Figure 15. The probability when the merger remnant is made of 27 GCs that the earliest merged GC0 in model 2 is drawn from the same population as all the others based on spatial distribution.

GC4 and GC5, have p -values $>1\%$ whereas GC9 has a low probability that it is drawn from the same population as the other three. Similarly when 20 GCs have merged GC3, GC4, GC12 and GC15, which have been merged for longest, have p -values >0.001 in tests between each other whereas GC19 has a p -value $<5 \times 10^{-6}$ that its stars are drawn from the same population as any of the others. When 27 GCs have merged GC3 and GC4 have a similar spatial distribution and GC19, GC22 and GC26 have low likelihoods of being drawn from the same population as GC3 and GC4.

At each time we find that the 6 to 8 most recently merged GCs have a low probability that they are drawn from the same population as earlier merged GCs based on their spatial distribution. When GCs have merged prior to this in the merger sequence their stars have a spatial distribution which is similar to that of the overall merger remnant. An illustration of this is shown in Figure 15. This shows the probability that the earliest merged GC, GC0, is drawn from the same population as each of the others when the merger remnant contains stars from 27 GCs. This p -value is generally ~ 0.2 to 0.5 but always $>1\%$ for all GCs up to GC18 and

then falls sharply from GC19 (probability, $p < 10^{-5}$) to GC26 (just merged). This implies that stars from a GC which has merged in the most recent 8 mergers could be distinguished by their spatial distribution but stars from a GC which underwent a prior merger could not.

Figure 16 shows the p -values laid out as before for all pairs of GCs at the end of the simulation in model 2. The lower right half of the figure shows the p -values for velocity distribution. These p -values are all $>10\%$ showing we cannot use their velocity distribution to distinguish stars from different GCs. The upper left half of the figure shows p -values for spatial distribution. The p -values of the last 6 to 8 GCs to merge when tested with one of the first 18 GCs to merge are low. p -values for GC0 to GC18 taken in pairs show higher likelihood that these GCs are drawn from the same population.

If we look for groups of GCs which all have p -values of $>10\%$ when tested with each other then we find two large groups made up of 11 and 7 GCs and three small groups of 3, 3 and 2 GCs. The two large groups are made up from the first 18 GCs to merge. If we set the p -value threshold at 1% we still find 2 large groupings made up of 15 and 6 GCs (again made up from the earlier GCs to merge) and two smaller made up of 3 and 2 GCs. This implies that if observations find kinematic substructure then it is not because of mergers.

3.3 Dependence of K-S results on number of observable data points

We have chosen, somewhat arbitrarily, 200 stars to compare our distributions. Given that we have simulations with ~ 40000 star particles representing each GC we could have used up to thousands of data points to perform our K-S tests. Though the profiles we have examined would not have changed by using more points it is true that using more points would result in lower p values for the same value of D . Observational uses of the K-S test are limited by the number of stars observed and so for our purposes we should ensure that we are performing our tests with values of N_p which are comparable to observations. Kućinskas, Dobrovolskas & Bonifacio (2014) perform their

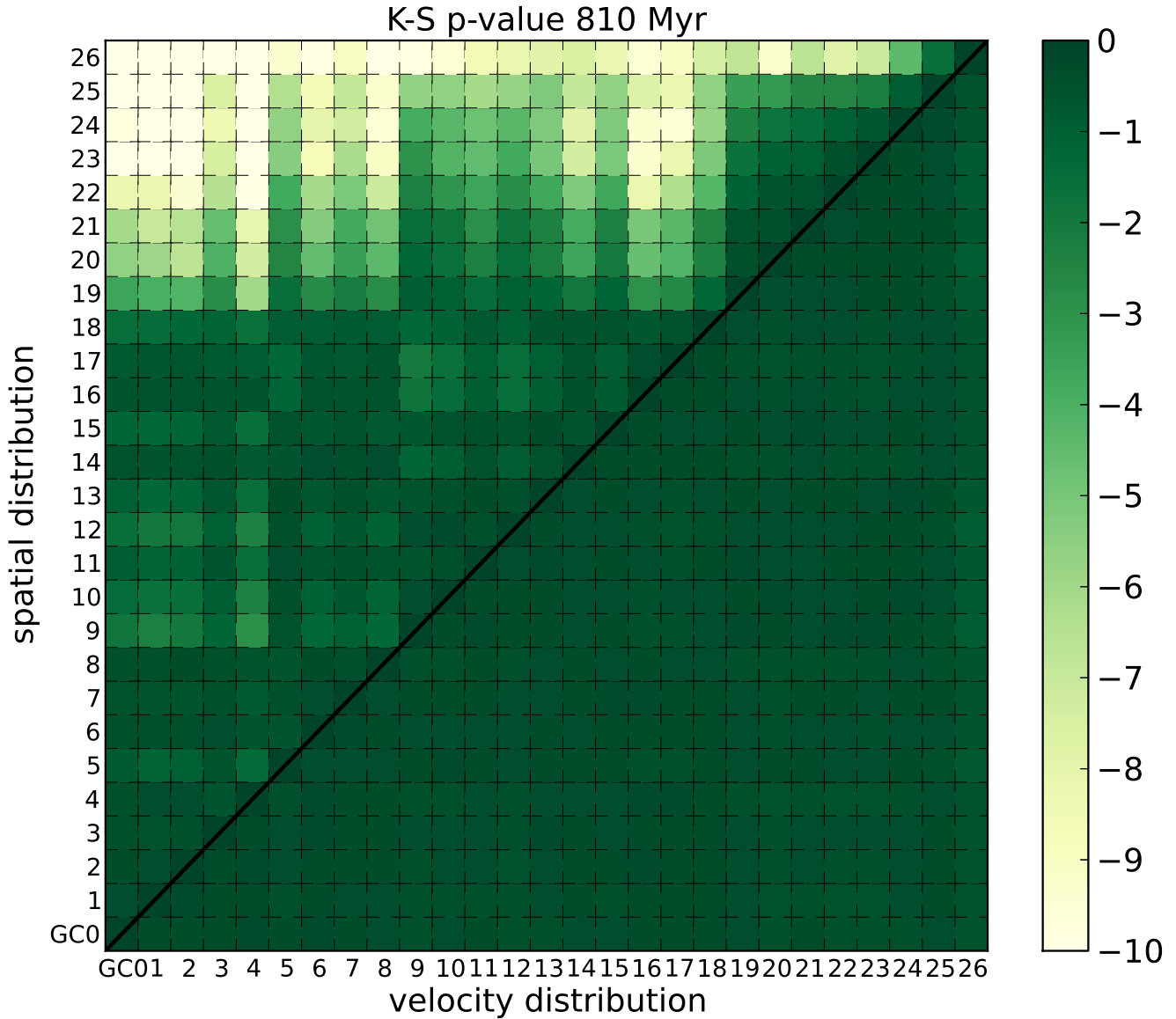


Figure 16. p -values for the cumulative spatial distribution of 200 stars within $4R_e$ at the end of the simulation for model 2, for all pairs of GCs. The p -value for any pair of GCs is found at the intersection of the appropriate row and column. The figure is colour coded so that high p -values are green and low p -values are yellow.

K-S tests on 101 main sequence turn-off stars in 47 Tuc meaning they are comparing subsamples with tens of stars. Lardo et al. (2011) used K-S tests to distinguish different populations of stars in the u , g , r SDSS bands. They compared samples containing from 10s to several hundred stars. In order to assess the effect of using larger numbers of stars we repeated some of our K-S tests again with 1000 stars.

Figure 17 shows the p -values as described in Section 3.1.3 but now with 1000 stars in each distribution. At 200 Myr the results are similar to the results with 200 stars. As previously GC2 is distinguishable by its spatial distribution. At 400 Myr however most GC pairs have a spatial p -value $< 10^{-6}$ and are now distinguishable by their spatial distribution. Only GC0/GC1 and GC2/GC3 have a p -value for their spatial distribution $> 1.5\%$. We see a similar effect at 1560 Myr though not quite as marked. However at this time

GC2, GC4 and GC5 are distinguishable by their spatial distribution with GC3, GC4 and GC5 having relatively high p -values that they are drawn from the same population. Increasing the number of stars has had a significant effect on our ability to identify different populations by their spatial distribution.

4 DISCUSSION

We have shown that the stars originating in individual GCs which merge can be difficult to identify from their spatial or velocity distributions with currently observable sample sizes. It is often the most recently merged GCs which are distinguishable by observations. Stars from the most recently merged few GCs have a low probability, based on

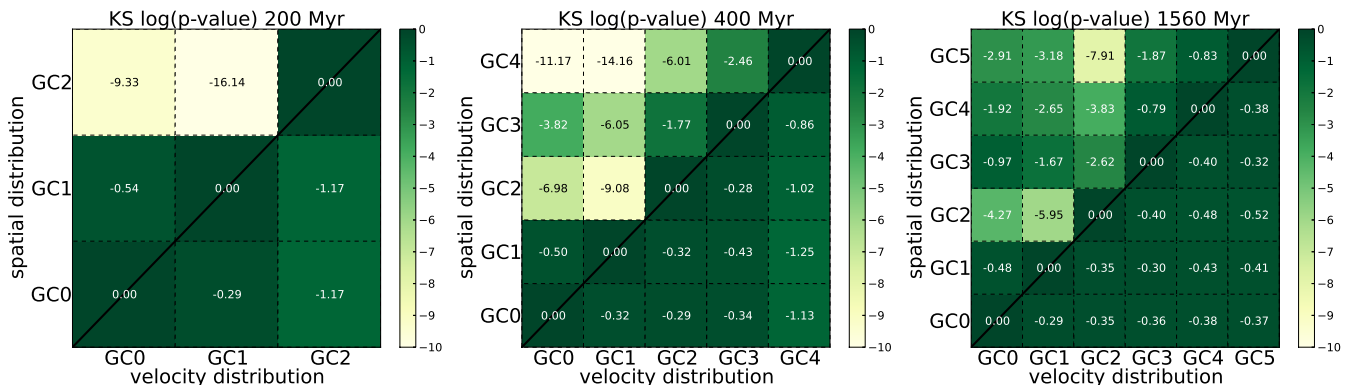


Figure 17. Model 1 \log_{10} of p -values for the cumulative spatial distribution of 1000 stars within $4R_e$ when the merger remnant contains 3 GCs (left), 5 GCs (middle) and 6 GCs (right) and cumulative absolute velocity distribution as seen by an observer viewing the system edge on to the average plane of the GCs’ initial orbits as in Figure 9. The p -value for any pair of GCs is found at the intersection of the appropriate row and column. The figure is colour coded so that high p -values are green and low p -values are yellow.

their spatial distribution that they are drawn from the same population as earlier merged GCs. However this probability increases quickly as more GCs merge and soon become spatially distributed and kinematically similar to the rest of the cluster.

Our simulations are examples of violent relaxation (Lynden-Bell 1967) where the final distribution of particles is the result of the star particles being scattered by the rapidly changing gravitational potential produced by a merger. Studies of violent relaxation in galaxy mergers have found that radial abundance and colour gradients can survive the mixing of stellar populations but that they are reduced (White 1980; Barnes 1988; Mihos & Hernquist 1994; Barnes 1996).

Our simulation remnants are collisionless, non-spherical systems. Merritt & Valluri (1996) found that collisionless mixing in triaxial potentials representative of elliptical galaxies occurs with characteristic times of 10–30 dynamical times. For our systems the dynamical time at $R_e \sim 5 \times 10^5$ yr giving a mixing time of 5 to 15 Myr. Valluri et al. (2007) studied the mechanisms responsible for mixing in collisionless mergers (in their case dark matter halos). They found that the mixing in phase space is driven by the exchange of energy and angular momentum at pericentric passage due to tidal shocks and dynamical friction. They find that in the merger remnant most particles retain a memory of their original kinetic energy and angular momentum but there are changes due to the tidal shocks. Importantly they do not find more large scale mixing in radius compared to an isolated halo and conclude that radial gradients in stellar properties such as metallicity can survive such mergers. This supposes that such gradients exist prior to a merger, which is very likely for galaxies. In the case of NSCs (and potentially GCs too) we would like to know if the merging of stellar systems composed of a single population can produce multiple populations distinguishable by their spatial and velocity profiles. If mono-abundance GCs merge to form NSCs they will retain some of their kinetic energy and angular momentum profiles. Stars from different merging GCs will have similar spatial and velocity distributions prior to the merger and retain these afterwards. Our results indicate that creating a merger remnant results in the stars from different GCs

having a similar spatial and velocity distributions except for recent mergers, implying that if our clusters were made up of distinct stellar populations they would be difficult to detect by their spatial and velocity distributions.

Kobayashi (2004) studied the chemodynamic evolution of elliptical galaxies following mergers and showed that metallicity gradients have the largest change when the galaxies are of comparable mass. They find that when the mass ratio of the two galaxies is more than 20% then the metallicity gradient change is $\gtrsim 0.5$ dex. Di Matteo et al. (2009) investigated dry mergers of early-type galaxies with a variety of properties using N -body simulations. They found that such mergers do flatten the metallicity gradient of the merger remnant but that ellipticals can retain their pre-merger metallicity gradient if one of the merging galaxies has a steep pre-merger slope. Should a small metallicity gradient exist in our merger remnant the repeated merging in our simulations would be likely to continually reduce any stellar population gradients making any remnant gradient hard to observe. Building a NSC from GCs would require early mergers to have mass ratios more than 20% maximising the reduction in the existing gradient.

From the globular clusters perspective, the characterisation of the process of mixing of different stellar populations plays a crucial role for the interpretation of the spatial and kinematical properties of present-day Galactic star clusters. The key physical driver of the mixing is represented by two-body collisional relaxation processes, which, during the course of the long-term dynamical evolution of the systems, may gradually erase any intrinsic difference in the spatial and kinematical distribution of different stellar populations. Within the formation scenario in which the asymptotic giant branch stars are the “polluters” contributing to enrich the gas from which the second generation is formed, Vesperini et al. (2013) have explored, by means of direct N -body simulations, the time-scales and the dynamics of the spatial mixing of two different populations, and their dependence on the initial concentration of the “second generation” stars. They found that the time-scale for complete mixing indeed depends on the initial concentration of the second generation, but that, in general, complete mixing is expected only for clusters in the late stages of

their evolution, after they have lost a significant fraction of their initial mass due to relaxation-driven processes. Such a theoretical investigation therefore supports the observational evidence that, in several present-day star clusters, different populations are characterised by distinguishable spatial distributions (with the helium-enriched population being the more centrally concentrated one). In particular, Kučinskas, Dobrovolskas & Bonifacio (2014) in a study of 47 Tuc found that a K-S test of the fractional distribution of the different generations of stars plotted against radius from the centre of the cluster gives a probability $p = 6.0 \times 10^{-7}$ that the primordial and chemically enriched distributions are drawn from the same population (for a total of 101 stars). K-S tests of the absolute radial velocities of the different stellar generations also give low probabilities that they are drawn from the same population ($p = 7.0 \times 10^{-7}$). We emphasise that K-S tests with a greater number of stars from mass components associated with specific GCs in our simulations find much higher likelihoods that they are drawn from the same population both for spatial and velocity distributions.

As for the globular clusters kinematical properties, it has been shown, again with the support of direct N -body simulations, that different populations may be characterised by different kinematical properties, as established by the effects of two-body relaxation process (see Section 4 in Bellini et al. 2015). In particular, it results that the diffusion from the innermost regions to the outer parts of the clusters of the most centrally concentrated population is associated with the growth of radial anisotropy in such a population, in agreement with recent observational studies of selected Galactic globular clusters (47 Tuc, Richer et al. (2013); NGC 2808, Bellini et al. (2015)). One additional question is related to the kinematic imprints (and their survival) of different formation scenarios for multiple stellar populations in GCs. Hénault-Brunet et al. (2015) have addressed such a question by using direct N -body simulations, and they found that different formation mechanisms show distinct kinematical signatures that can persist for a Hubble time. In summary, in the context of the formation and dynamical evolution of globular clusters, there is convincing evidence, mostly based on N -body models, that spatial and kinematical differences, either intrinsically associated with the formation scenarios or induced by collisional relaxation processes, may persist for several half-mass relaxation times.

Bearing in mind the fundamental differences between the formation scenarios (and the intrinsic nature) of globular clusters and nuclear star clusters, we have performed an investigation of the structural and kinematical properties of the mass components associated with different proto-clusters, progressively merged to form a single central stellar systems. Motivated by specific cases of peculiar star clusters which, in light of their chemical and dynamical complexity, have been suggested to be stripped nuclei of dwarf galaxies (e.g., M 54, ω Cen), we wished to assess the existence and persistence of any spatial or dynamical signature associated with the merger histories considered in our two simulations. Our analysis shows that such a differentiation is difficult with currently available numbers of observations if NSCs formed by merging alone, except for recent mergers.

5 ACKNOWLEDGEMENTS

Simulations in this paper were carried out on the COSMOS Shared Memory system at DAMTP, University of Cambridge operated on behalf of the STFC DiRAC HPC Facility. This equipment is funded by BIS National E-infrastructure capital grant ST/J005673/1 and STFC grants ST/H008586/1, ST/K00333X/1. DRC and VPD were supported by STFC Consolidated grant #ST/J001341/1. We made use of pynbody (<https://github.com/pynbody/pynbody>) in our analysis for this paper. ALV acknowledges support from the Royal Commission for the Exhibition of 1851. We would like to acknowledge the Lorentz Centre in Leiden which hosted the meeting “Nuclear Star Clusters in Galaxies, and the Role of the Environment”, 30 June to 4 July 2014, where discussions stimulated our ideas set forth in this paper.

REFERENCES

- Amaro-Seoane P., Konstantinidis S., Brem P., Catelan M., 2013, MNRAS, 435, 809
 Anderson J., van der Marel R. P., 2010, ApJ, 710, 1032
 Antonini F., 2013, ApJ, 763, 62
 Antonini F., Capuzzo-Dolcetta R., Mastrobuono-Battisti A., Merritt D., 2012, ApJ, 750, 111
 Barnes J., 1996, in IAU Symposium, Vol. 171, New Light on Galaxy Evolution, Bender R., Davies R. L., eds., p. 191
 Barnes J. E., 1988, ApJ, 331, 699
 Bastian N., 2015, ArXiv e-prints
 Bastian N., Lamers H. J. G. L. M., de Mink S. E., Longmore S. N., Goodwin S. P., Gieles M., 2013, MNRAS, 436, 2398
 Bekki K., 2007, PASA, 24, 77
 Bekki K., Norris J. E., 2006, ApJL, 637, L109
 Bekki K., Yong D., 2012, MNRAS, 419, 2063
 Bellini A. et al., 2015, ApJL, 810, L13
 Bianchini P., Varri A. L., Bertin G., Zocchi A., 2013, ApJ, 772, 67
 Binney J., 2005, MNRAS, 363, 937
 Böker T., Laine S., van der Marel R. P., Sarzi M., Rix H.-W., Ho L. C., Shields J. C., 2002, AJ, 123, 1389
 Briggs F. H., 1990, ApJ, 352, 15
 Capuzzo-Dolcetta R., 1993, ApJ, 415, 616
 Capuzzo-Dolcetta R., Miocchi P., 2008a, ApJ, 681, 1136
 Capuzzo-Dolcetta R., Miocchi P., 2008b, MNRAS, 388, L69
 Carollo C. M., Stiavelli M., de Zeeuw P. T., Mack J., 1997, AJ, 114, 2366
 Carretta E., 2015, ApJ, 810, 148
 Carretta E. et al., 2010a, A&A, 520, A95
 Carretta E. et al., 2010b, ApJL, 714, L7
 Carretta E., Lucatello S., Gratton R. G., Bragaglia A., D’Orazi V., 2011, A&A, 533, A69
 Carson D. J., Barth A. J., Seth A. C., den Brok M., Cappellari M., Greene J. E., Ho L. C., Neumayer N., 2015, AJ, 149, 170
 Catelan M., 1997, ApJL, 478, L99
 Cen R., 2001, ApJ, 560, 592
 Cordero M. J., Pilachowski C. A., Johnson C. I., McDonald I., Zijlstra A. A., Simmerer J., 2014, ApJ, 780, 94
 Côté P. et al., 2006, ApJS, 165, 57

- Da Costa G. S., Held E. V., Saviane I., Gullieuszik M., 2009, *ApJ*, 705, 1481
- D'Antona F., Vesperini E., D'Ercole A., Ventura P., Milone A. P., Marino A. F., Tailo M., 2016, *MNRAS*
- De Lorenzi F., Hartmann M., Debattista V. P., Seth A. C., Gerhard O., 2013, *MNRAS*, 429, 2974
- de Mink S. E., Pols O. R., Langer N., Izzard R. G., 2009, *A&A*, 507, L1
- Debattista V. P., Sellwood J. A., 2000, *ApJ*, 543, 704
- D'Ercole A., D'Antona F., Carini R., Vesperini E., Ventura P., 2012, *MNRAS*, 423, 1521
- D'Ercole A., D'Antona F., Ventura P., Vesperini E., McMillan S. L. W., 2010, *MNRAS*, 407, 854
- D'Ercole A., Vesperini E., D'Antona F., McMillan S. L. W., Recchi S., 2008, *MNRAS*, 391, 825
- Di Matteo P., Pipino A., Lehnert M. D., Combes F., Semelin B., 2009, *A&A*, 499, 427
- D'Souza R., Rix H.-W., 2013, *MNRAS*, 429, 1887
- Emsellem E., van de Ven G., 2008, *ApJ*, 674, 653
- Ferraro F. R. et al., 2009, *Nature*, 462, 483
- Figer D. F., McLean I. S., Morris M., 1999, *ApJ*, 514, 202
- Figer D. F. et al., 2002, *ApJ*, 581, 258
- Georgiev I. Y., Böker T., 2014, *MNRAS*, 441, 3570
- Gnedin O. Y., Ostriker J. P., 1997, *ApJ*, 474, 223
- Gnedin O. Y., Ostriker J. P., Tremaine S., 2014, *ApJ*, 785, 71
- Gratton R. G., Carretta E., Bragaglia A., 2012, *A&A Rev.*, 20, 50
- Harris W. E., 1997, *VizieR Online Data Catalog*, 7202, 0
- Hartmann M., Debattista V. P., Seth A., Cappellari M., Quinn T. R., 2011, *MNRAS*, 418, 2697
- Hénault-Brunet V., Gieles M., Agertz O., Read J. I., 2015, *MNRAS*, 450, 1164
- Hernquist L., 1990, *ApJ*, 356, 359
- Ibata R. et al., 2009, *ApJL*, 699, L169
- Kobayashi C., 2004, *MNRAS*, 347, 740
- Kučinskas A., Dobrovolskas V., Bonifacio P., 2014, *A&A*, 568, L4
- Lanzoni B. et al., 2010, *ApJ*, 717, 653
- Lapenna E., Mucciarelli A., Lanzoni B., Ferraro F. R., Dalessandro E., Origlia L., Massari D., 2014, *ApJ*, 797, 124
- Lardo C., Bellazzini M., Pancino E., Carretta E., Bragaglia A., Dalessandro E., 2011, *A&A*, 525, A114
- Lardo C. et al., 2015, *A&A*, 573, A115
- Lee Y.-W., Joo J.-M., Sohn Y.-J., Rey S.-C., Lee H.-C., Walker A. R., 1999, *Nature*, 402, 55
- Long K. S., Charles P. A., Dubus G., 2002, *ApJ*, 569, 204
- Lynden-Bell D., 1967, *MNRAS*, 136, 101
- Lyubenova M. et al., 2013, *MNRAS*, 431, 3364
- Mackey A. D., Gilmore G. F., 2003, *MNRAS*, 340, 175
- Marino A. F. et al., 2016, *MNRAS*
- Marino A. F. et al., 2015, *MNRAS*, 450, 815
- Marino A. F., Milone A. P., Piotto G., Villanova S., Bedin L. R., Bellini A., Renzini A., 2009, *A&A*, 505, 1099
- Marino A. F. et al., 2011, *A&A*, 532, A8
- Marks M., Kroupa P., 2010, *MNRAS*, 406, 2000
- Massari D. et al., 2014, *ApJ*, 795, 22
- Mastrobuono-Battisti A., Perets H. B., 2013, *ApJ*, 779, 85
- McLaughlin D. E., van der Marel R. P., 2005, *ApJS*, 161, 304
- Merritt D., Valluri M., 1996, *ApJ*, 471, 82
- Meylan G., Mayor M., Duquenois A., Dubath P., 1995, *A&A*, 303, 761
- Mihos J. C., Hernquist L., 1994, *ApJ*, 427, 112
- Milosavljević M., 2004, *ApJL*, 605, L13
- Miocchi P., 2010, *A&A*, 514, A52
- Miocchi P., Capuzzo Dolcetta R., Di Matteo P., Vicari A., 2006, *ApJ*, 644, 940
- Mucciarelli A., Lapenna E., Massari D., Ferraro F. R., Lanzoni B., 2015, *ApJ*, 801, 69
- Noyola E., Gebhardt K., Bergmann M., 2008, *ApJ*, 676, 1008
- Origlia L. et al., 2011, *ApJL*, 726, L20
- Pancino E., Bellazzini M., Marinoni S., 2013, *Mem. Soc. Astron. Italiana*, 84, 83
- Perets H. B., Mastrobuono-Battisti A., 2014, *ApJL*, 784, L44
- Pfuhl O. et al., 2011, *ApJ*, 741, 108
- Piotto G. et al., 2015, *AJ*, 149, 91
- Portaluri E., Corsini E. M., Morelli L., Hartmann M., Dalla Bontà E., Debattista V. P., Pizzella A., 2013, *MNRAS*, 433, 434
- Prantzos N., Charbonnel C., 2006, *A&A*, 458, 135
- Renzini A. et al., 2015, *MNRAS*, 454, 4197
- Richer H. B., Heyl J., Anderson J., Kalirai J. S., Shara M. M., Dotter A., Fahlman G. G., Rich R. M., 2013, *ApJL*, 771, L15
- Rossa J., van der Marel R. P., Böker T., Gerssen J., Ho L. C., Rix H.-W., Shields J. C., Walcher C.-J., 2006, *AJ*, 132, 1074
- Sarajedini A., Layden A. C., 1995, *AJ*, 109, 1086
- Sellwood J. A., 2008, *ApJ*, 679, 379
- Sellwood J. A., Debattista V. P., 2009, *MNRAS*, 398, 1279
- Seth A. C., Blum R. D., Bastian N., Caldwell N., Debattista V. P., 2008, *ApJ*, 687, 997
- Seth A. C., Dalcanton J. J., Hodge P. W., Debattista V. P., 2006, *AJ*, 132, 2539
- Siegel M. H. et al., 2007, *ApJL*, 667, L57
- Siegel M. H. et al., 2011, *ApJ*, 743, 20
- Sollima A., Bellazzini M., Smart R. L., Correnti M., Pancino E., Ferraro F. R., Romano D., 2009, *MNRAS*, 396, 2183
- Stadel J. G., 2001, PhD thesis, UNIVERSITY OF WASHINGTON
- Tremaine S. D., Ostriker J. P., Spitzer, Jr. L., 1975, *ApJ*, 196, 407
- Turner M. L., Côté P., Ferrarese L., Jordán A., Blakeslee J. P., Mei S., Peng E. W., West M. J., 2012, *ApJS*, 203, 5
- Valluri M., Vass I. M., Kazantzidis S., Kravtsov A. V., Bohn C. L., 2007, *ApJ*, 658, 731
- van de Ven G., van den Bosch R. C. E., Verolme E. K., de Zeeuw P. T., 2006, *A&A*, 445, 513
- van den Bergh S., 1996, *ApJL*, 471, L31
- van der Marel R. P., Anderson J., 2010, *ApJ*, 710, 1063
- Ventura P., D'Antona F., Mazzitelli I., Gratton R., 2001, *ApJL*, 550, L65
- Vesperini E., McMillan S. L. W., D'Antona F., D'Ercole A., 2013, *MNRAS*, 429, 1913
- Walcher C. J., Böker T., Charlot S., Ho L. C., Rix H.-W., Rossa J., Shields J. C., van der Marel R. P., 2006, *ApJ*, 649, 692
- Walcher C. J. et al., 2005, *ApJ*, 618, 237

- Watkins L. L., van der Marel R. P., Bellini A., Anderson J., 2015, *ApJ*, 812, 149
White S. D. M., 1980, *MNRAS*, 191, 1P
Wrobel J. M., Greene J. E., Ho L. C., 2011, *AJ*, 142, 113
Yong D. et al., 2014, *MNRAS*, 441, 3396